Supporting Information

A 2D few-layer iron phosphosulfide: self-buffer heterophase structure induced by irreversible breakage of P-S bonds for high-performance lithium/sodium storage

Chao-Ying Fan,[ab] *Xiao-Hua Zhang,*[a] *Yan-Hong Shi,*[a] *Hai-Yang Xu,*[b] *Jing-Ping Zhang,*[*a] *Xing-Long Wu*[*a]

[a]Faculty of Chemistry, National & Local United Engineering Lab for Power Battery, Northeast Normal University, Changchun, Jilin 130024, P. R. China.
[b]Key Laboratory for UV Light-Emitting Materials and Technology, Northeast Normal University, Ministry of Education, Changchun, Jilin 130024, P. R. China
*E-mail: xinglong@nenu.edu.cn; jpzhang@nenu.edu.cn

Experimental Section

The preparation of e-$FePS_3$: First, the iron powder (Macklin, AR), sulfur powder (Aladdin, AR), and red phosphorus (Aladdin, AR) with stoichiometric ratio were *co*-heated in the vacuum sealed tube at 500 ^{o}C for 6 days to obtain b-$FePS_3$. Next, the b-$FePS_3$ was exfoliated through the ultrasound in organic solvent for 3 h. In order to acquire optimum exfoliation effect, eight kinds of different solvents namely deionized water (H_2O), n-hexane, *N*, *N*-dimethylformamide (DMF), acetone, *N*-methyl pyrrolidone (NMP), ethanol, acetylacetone, and isopropanol (IPA) were chosen. In addition, four different concentrations of b-$FePS_3$ in the solvent (0.5, 1, 2, and 4 mg mL^{-1}) was prepared to explore the effect on exfoliation. After the ultrasound, the low-speed centrifugation at 3000 rpm was conducted for 15 min to remove the deposition which was not exfoliated. As a result, the uniform suspension of e-$FePS_3$ was obtained.

The preparation of rGO-$FePS_3$ composite: The graphene oxide (GO) suspension was first synthesized by modified Hummer's method.[1] And then, 25 mg GO (4.6 mg mL^{-1}) was added into the e-$FePS_3$ suspension and mixed uniformly by stirring. Subsequently, 100 μL hydrazine hydrate ($N_2H_4 \cdot H_2O$) was added into the mixture to reduce GO for 24 h under the continuous stir. Next, the product was cleaned with deionized water several times and lyophilized at -50 ^{o}C for 12 h.

Material characterizations: The composition of the samples was explored through powder XRD using X-ray diffractometer with Cu Kα radiation (λ=1.5418 Å) (D8 Bruker). The Raman spectrometer with an excitation laser beam wavelength of 633 nm (JY HR-800, HORIBA JOBIN YVON) was used to further analysis the structure of b-$FePS_3$ and rGO-$FePS_3$. The information of chemical bonding of b-$FePS_3$ and rGO-$FePS_3$ was acquired through infrared

spectrometer (Nicolet 6700-FTIR, Thermo-Scientific). The composition and electronic state of rGO-$FePS_3$ was measured by XPS study (ESCALAB 250, Thermo). The AFM images were recorded in tapping mode with a Digital Instruments NanoScopeIII under ambient conditions. The SEM with energy dispersive spectrometer (Hitachi SU8000) and TEM (JEOL-2100F) were performed to probe the morphology and elemental mapping of b-$FePS_3$, e-$FePS_3$ and rGO-$FePS_3$.

Electrochemical measurement: Standard CR2032-type coin cells were assembled in Ar-filled glove box with oxygen and water value lower than 0.01 ppm. The work electrode was prepared by uniformly mixing 70% active materials (b-$FePS_3$ or rGO-$FePS_3$), 20% acetylene black, and 10% polyvinylidene fluoride in the NMP solvent, and then, the slurry was evenly coated on Cu foil and dried at 60 ^{o}C for 24 h. For LIBs, the lithium foil served as the counter electrode and reference electrode. The electrolyte was composed of 1 M $LiPF_6$ dissolved into ethylene carbonate (EC) and dimethyl carbonate (DMC) (1:1 by volume). For SIBs, the sodium foil acted as counter electrode and reference electrode. 1 M $NaClO_4$ in EC and propylene carbonate (PC) (1:1 by volume) was the electrolyte with 5 wt% fluoroethylene carbonate (FEC) as additive. Galvanostatic tests of LIBs and SIBs were conducted through LAND CT2001A battery-testing instrument in the voltage range from 0.01-3.0 V vs. Li/Li^+ or Na/Na^+. The CV measurement was carried out using the electrochemical station (CHI750E) at the scan rates of 0.01-2.0 mV s^{-1} within the voltage range from 0.01-3.0 V. The electrochemical kinetics of electrodes was investigated through the EIS test at different cycles using the CHI750E. The amplitude of the sine perturbation signal was 5 mV and the frequency was scanned from the highest (10^5 Hz) to lowest (0.01 Hz).

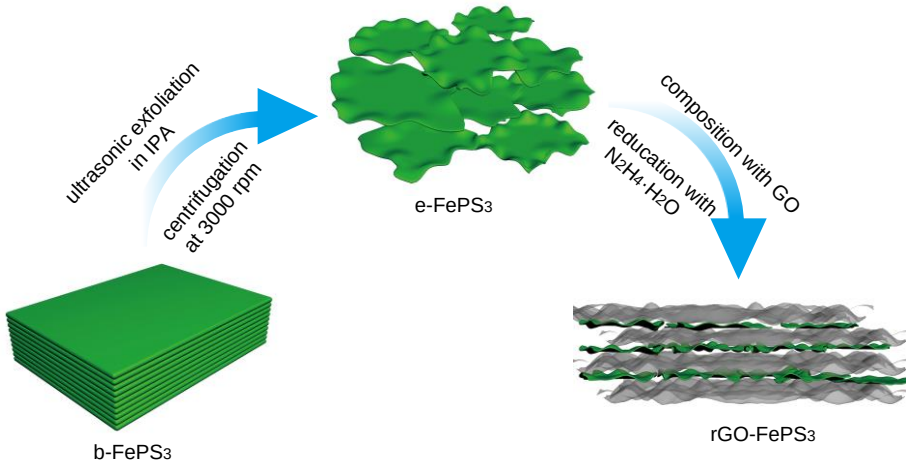

Fig. S1 The graphical illustration of the preparation of rGO-$FePS_3$ composite.

Table S1 The performance comparison of rGO-$FePS_3$ electrode with other binary metal sulfides and phosphides reported in the literatures for lithium storage.

	composites	Current density (A g^{-1})	Cycle number	Reversible capacity (mA h g^{-1})	Publish year
Metal phosphosulfides	rGO-$FePS_3$	0.1 1.0 8.0	120 1000 55	842.7 569.8 269.8	This work
Metal sulfides	MoS_2@ADC[2]	0.1 1	50 40	800 400	2016
	RGO-$NiCo_2S_4$[3]	0.5 1.6	84 50	903 489.3	2018
	ZnS-NPC[4]	0.1 4.0	200 50	1067.4 364.6	2017
	Co-Zn-S@N-S-C-CNT[5]	0.1 1	250 500	769 734	2016
	MoS_2/SnS_2-GS[6]	0.75 3.8	200 50	772 456	2017
	$Sn_{0.91}Co_{0.19}S_2$[7]	0.1 10	60 120	730 487.1	2017
	3D porous interconnected SnS@C[8]	1 10	300 15	535 329	2015
	NiS nanaoprisms/graphene[9]	0.07 5	200 50	622 141	2016
	$SnSe_{0.5}S_{0.5}$/C[10]	0.2 0.5 5	150 1000 70	785 625 389	2017
	C@FeNi-S[11]	0.18 1.5 2.2	200 1000 65	851.3 484.7 346.1	2017
metal phosphides	$Fe_xNi_{2-x}P$-C[12]	0.1 2.0	400 50	775 360	2018
	$ZnGeP_2$/C[13]	0.2 3.0	100 50	807 665	2017
	Hollow CoP NPs[14]	0.18 4.45	100 50	630 256	2013
	H-FeP@C@GR[15]	0.2 0.5 8.0	100 300 60	771 542 482	2017
	$Ni_{12}P_5$@C/GNS[16]	0.1 2.0	100 200	900 237.3	2017
	Ni_2P⊂pGN[17]	0.1 0.3 5.0	250 500 70	511 457 246	2017
	Ni_2P NPs@GSs[18]	0.1 5.4	200 280	625 410	2015
	Ni2P/$NiS_{0.66}$@C[19]	0.1 0.4 4.0	200 500 70	450 423.2 225	2017

Table S2 The performance comparison of rGO-$FePS_3$ electrode with other binary metal sulfides and phosphides reported in the literatures for sodium storage.

	composite	Current density (A g^{-1})	Cycle number	Reversible capacity (mA h g^{-1})	Publish year
Metal phosphosulfides	rGO-$FePS_3$	0.05 5.0	300 50	243.8 152.6	This work
Metal sulfides	ZnS/NPC[4]	0.1 1.0 4.0	100 1000 45	370.6 289.2 182.4	2017
	CL-C/FeS[20]	1.0 5.0	200 60	265 65	2017
	ZnS-Sb_2S_3@C[21]	0.1 0.8	120 40	630 390.6	2017
	3D porous interconnected SnS@C[8]	1.0 10	300 15	266 145	2015
	RGO-$NiCo_2S_4$[3]	0.05 0.8	70 50	530.2 221.7	2018
	Ni_3S_2 on Ni foam[22]	0.05 0.8	100 50	315.3 187.5	2016
	VS_2-SNSs[23]	0.2 10	100 30	245 180	2017
	Bi_2S_3 nanorods[24]	0.1 2.0	40 35	322 264	2016
Metal phosphides	H-FeP@C@GR[15]	0.1 1.6	250 50	400 237	2017
	Cu_4SnP_{10}/MWCNTs[25]	0.1 1.0	100 100	512 325	2017
	Ni_2P⊂pGN[17]	0.2 2.0	100 90	161 101	2017
	Co_2P-3D PNC[26]	0.05 3.0	100 100	306 179	2017
	RGO@CoP@C-FeP[27]	0.1 2.0	200 50	456.2 341.2	2017
	Sn_4P_3 NSs[28]	0.2 1.0	250 25	303 300	2017
	CoP@C-RGO-NF[29]	0.1 1.6	100 60	473.1 155	2017
	MoP Nanorods[30]	0.1 1.6	800 60	395.5 115.6	2017
	$Ni_{12}P_5$@C/GNS[16]	0.1 2.0	500 60	164.8 105.6	2017

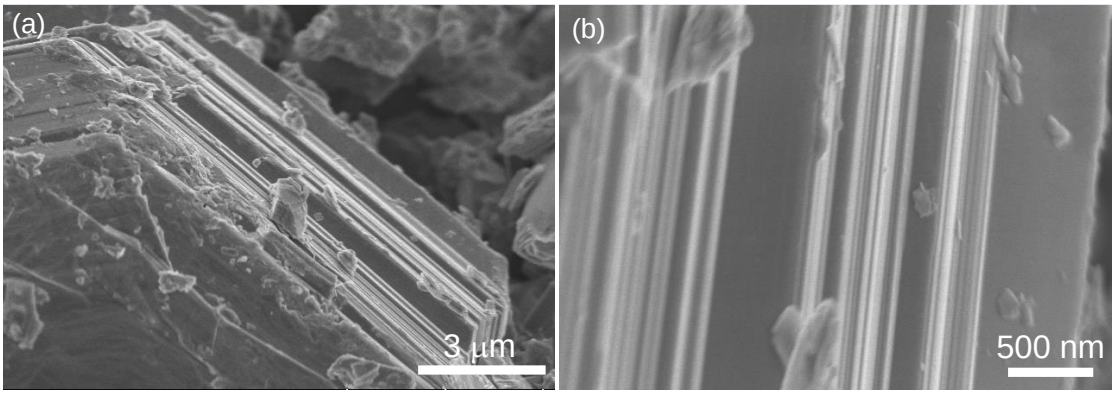

Fig. S2 (a) Low- and (b) high-resolution SEM images of b-$FePS_3$.

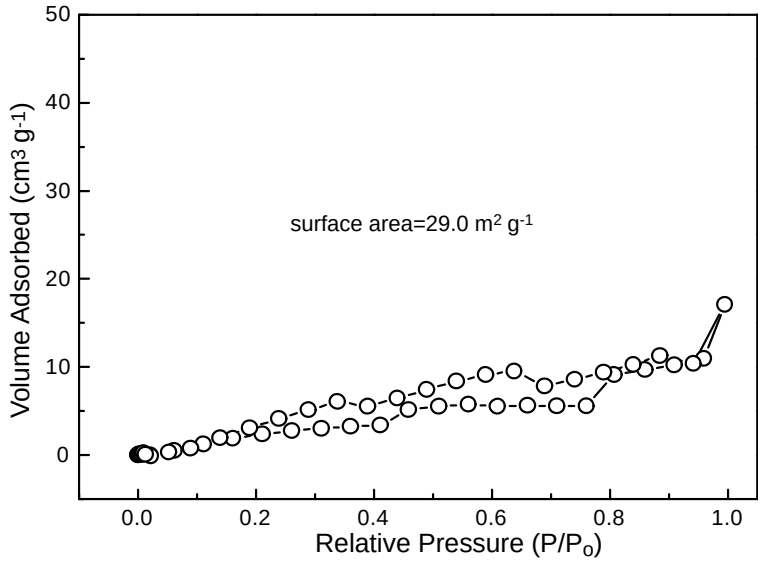

Fig. S3 N_2 adsorption-desorption isothermal curve of the b-$FePS_3$.

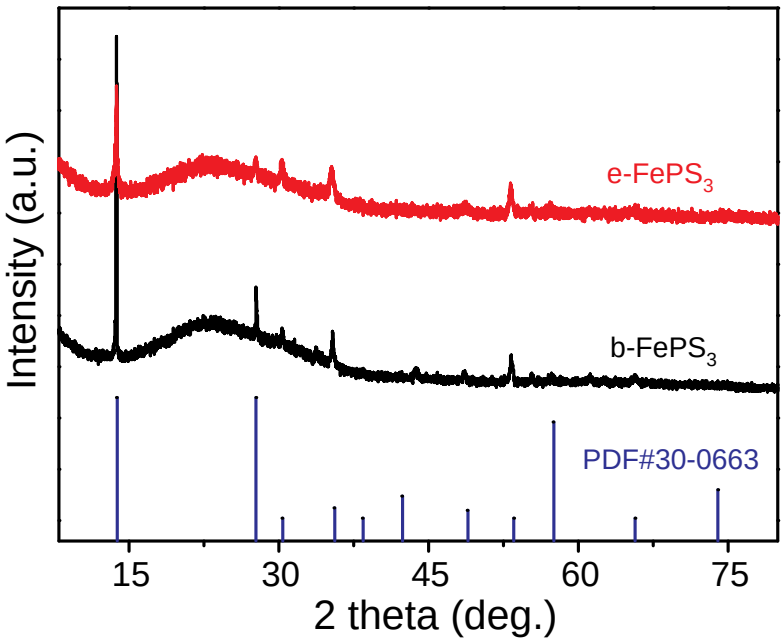

Fig. S4 XRD patterns of b-$FePS_3$ and e-$FePS_3$ with corresponding PDF pattern (PDF#30-0663).

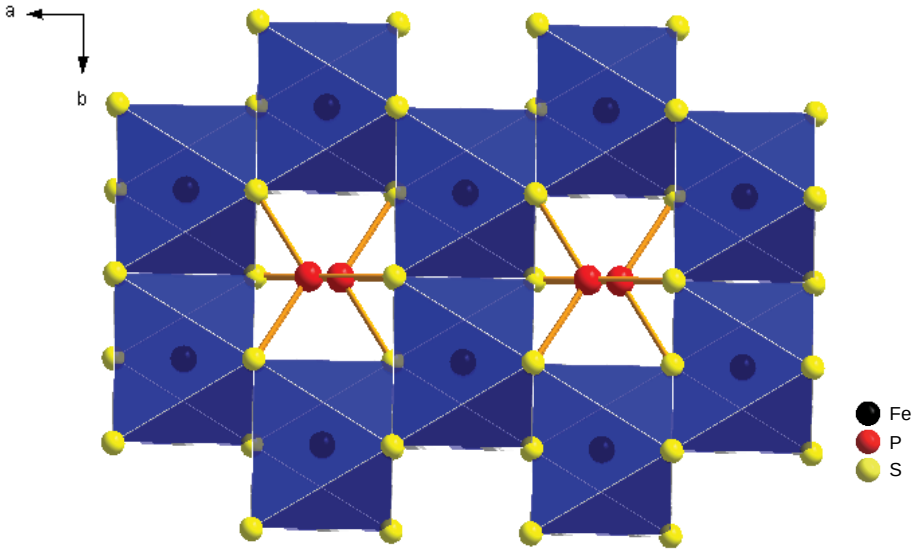

Fig. S5 Side view for the crystal structure of $FePS_3$.

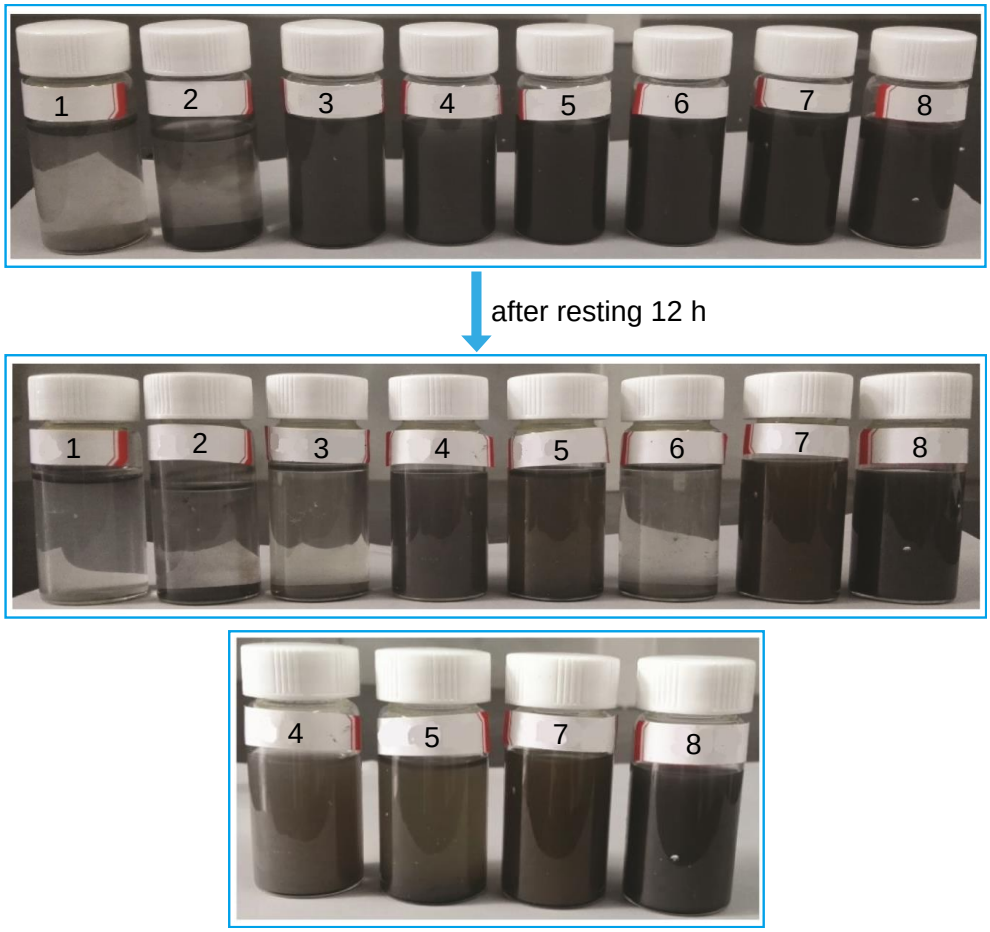

Fig. S6 Exfoliation of the b-$FePS_3$ at various solvents. Typical optical images of b-$FePS_3$ after the ultrasound in (1) H_2O, (2) n-hexane, (3) DMF, (4) acetone, (5) NMP, (6) ethanol, (7) acetylacetone, and (8) IPA solvents for 3 h with the concentration of 1 mg mL^{-1}, and then rest for 12 h.

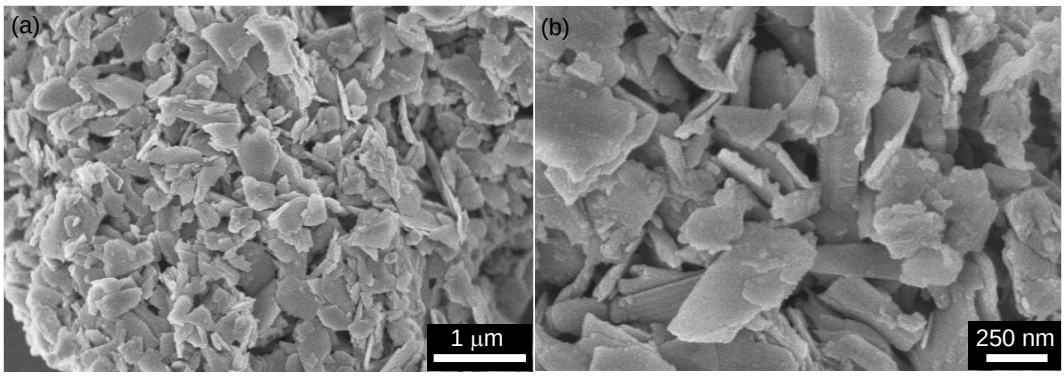

Fig. S7 (a) Low- and (b) high-resolution SEM images of e-$FePS_3$ obtained by ultrasound of b-$FePS_3$ in the IPA solvent with the concentration of 1 mg mL^{-1}.

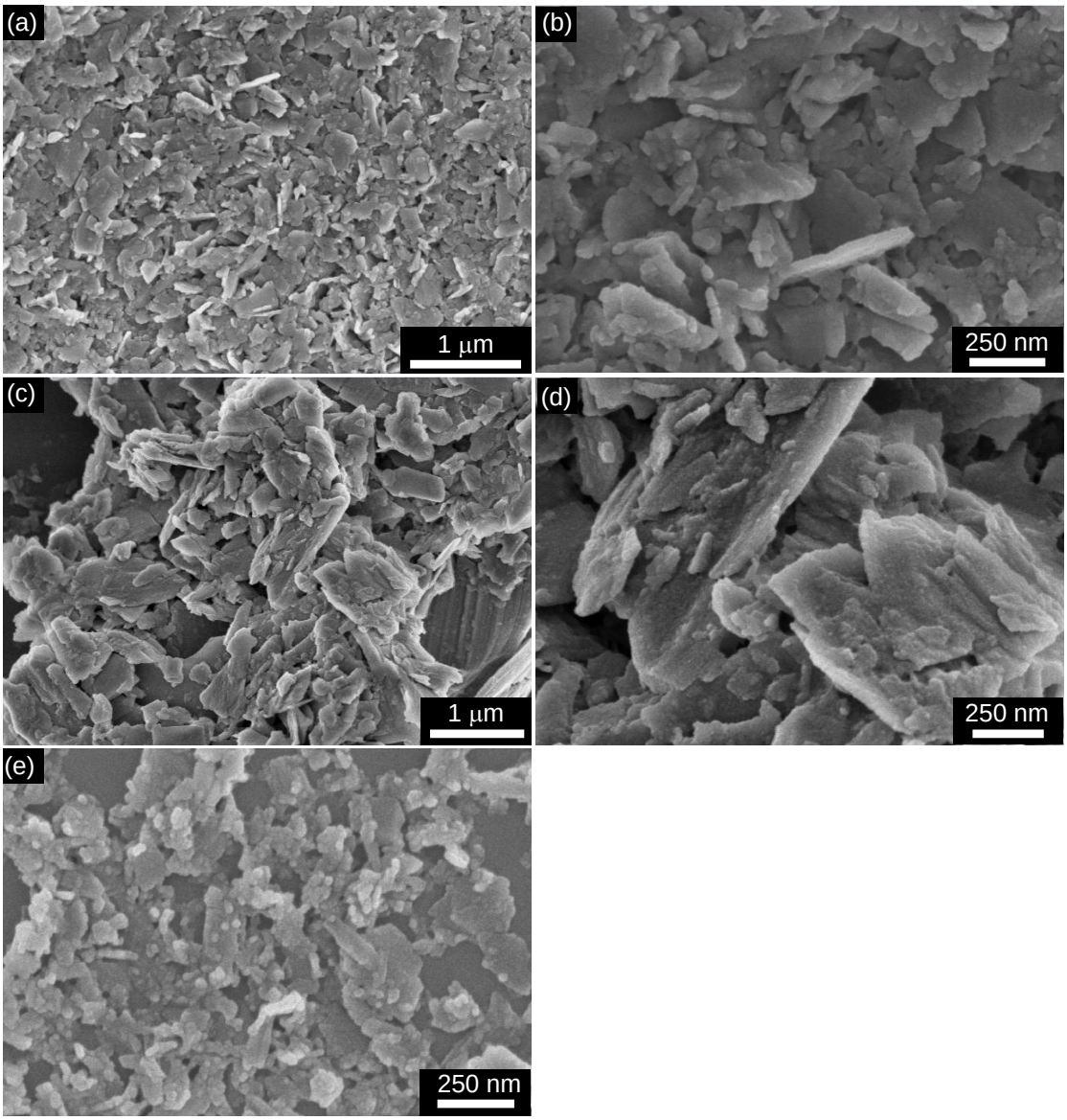

Fig. S8 SEM images of e-$FePS_3$ obtained by ultrasound of b-$FePS_3$ in the IPA solvent with the concentration of (a, b) 2 mg mL^{-1}, (c, d) 4 mg mL^{-1}, and (e) 0.5 mg mL^{-1}.

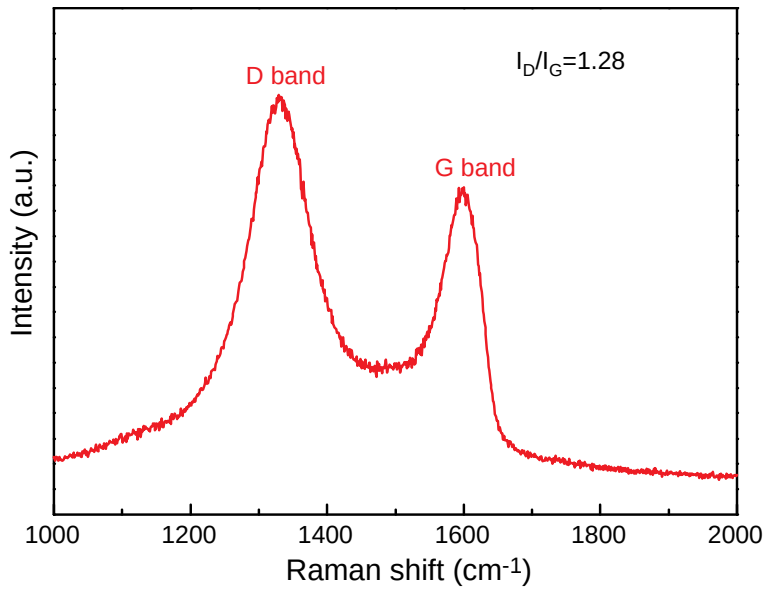

Fig. S9 Raman spectrum of rGO-$FePS_3$ in the range from 1000 to 2000 cm^{-1}.

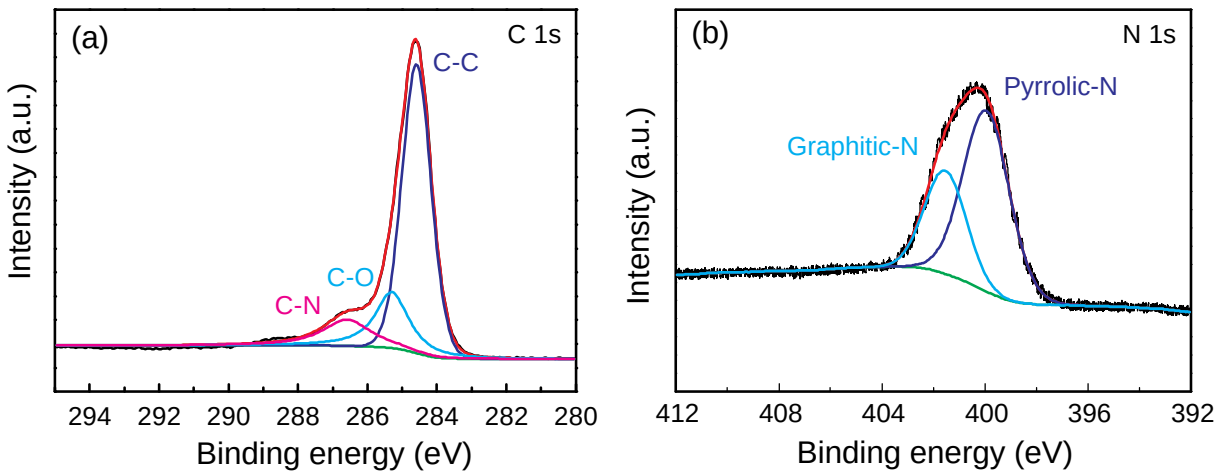

Fig. S10 High-resolution (a) C 1s and (b) N 1s XPS spectra of rGO-$FePS_3$.

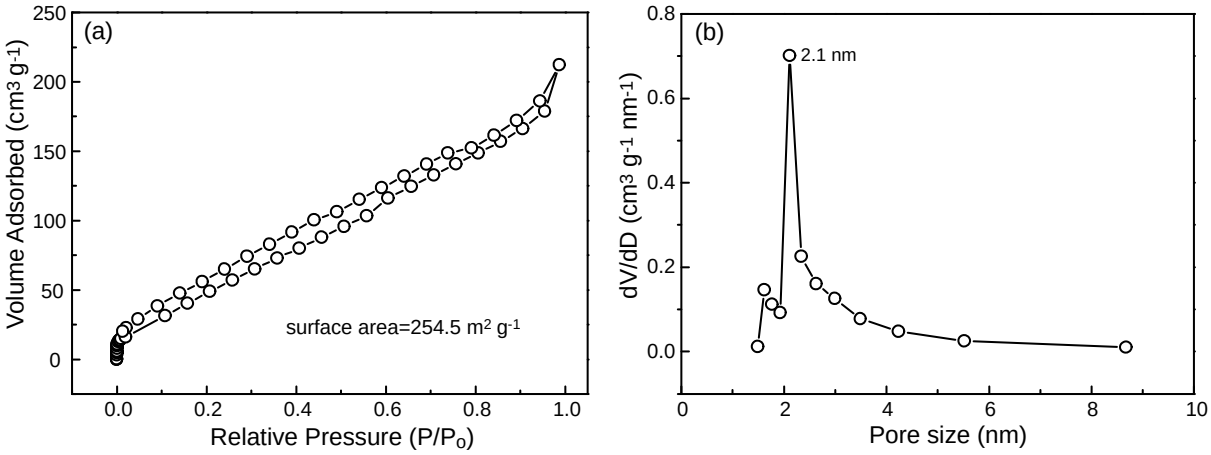

Fig. S11 (a) N_2 adsorption-desorption isothermal and (b) pore-size distribution curves of the rGO-$FePS_3$.

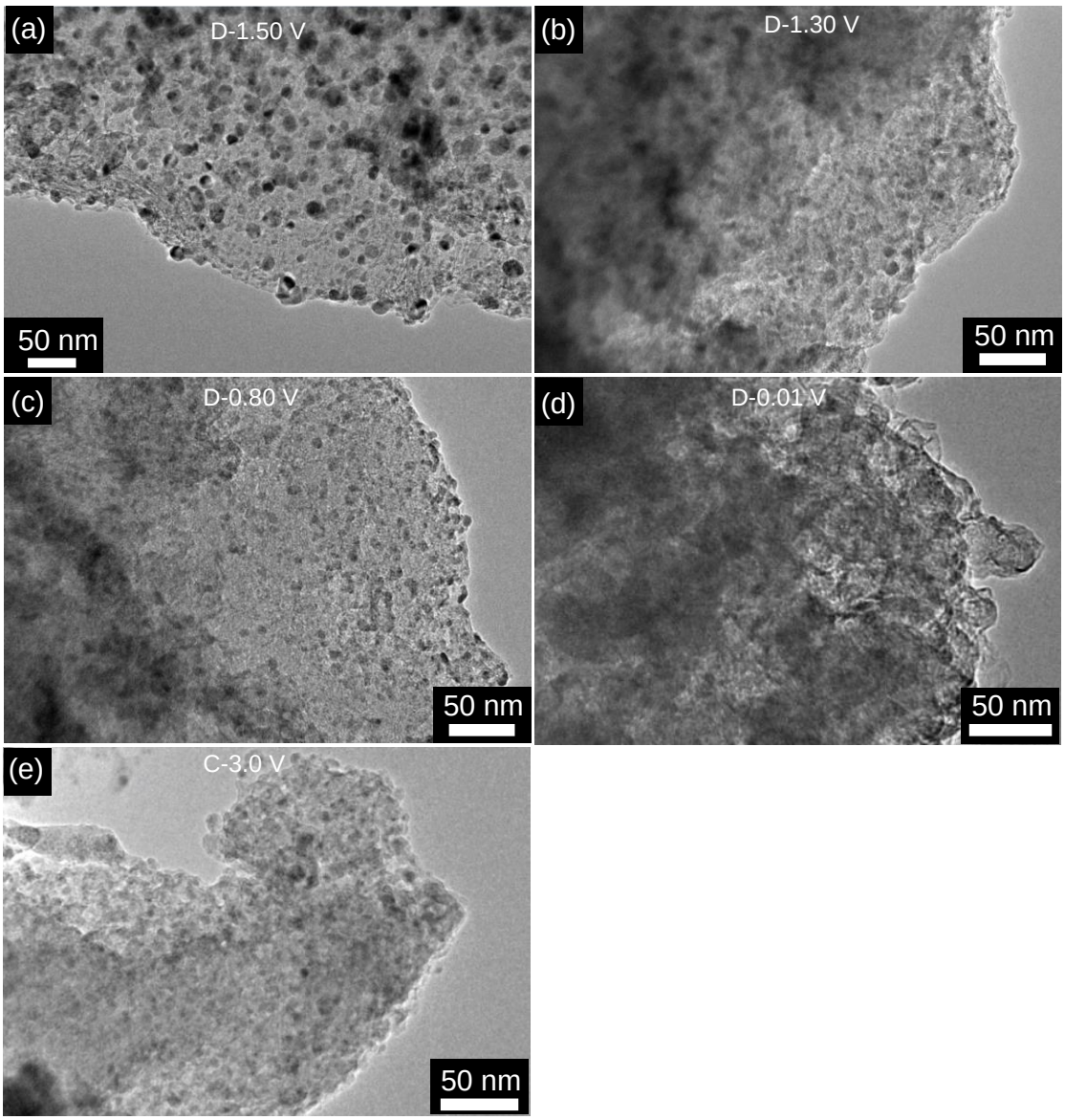

Fig. S12 Ex-situ TEM images of rGO-$FePS_3$ electrode in LIBs at selected charge-discharge states during the first cycle.

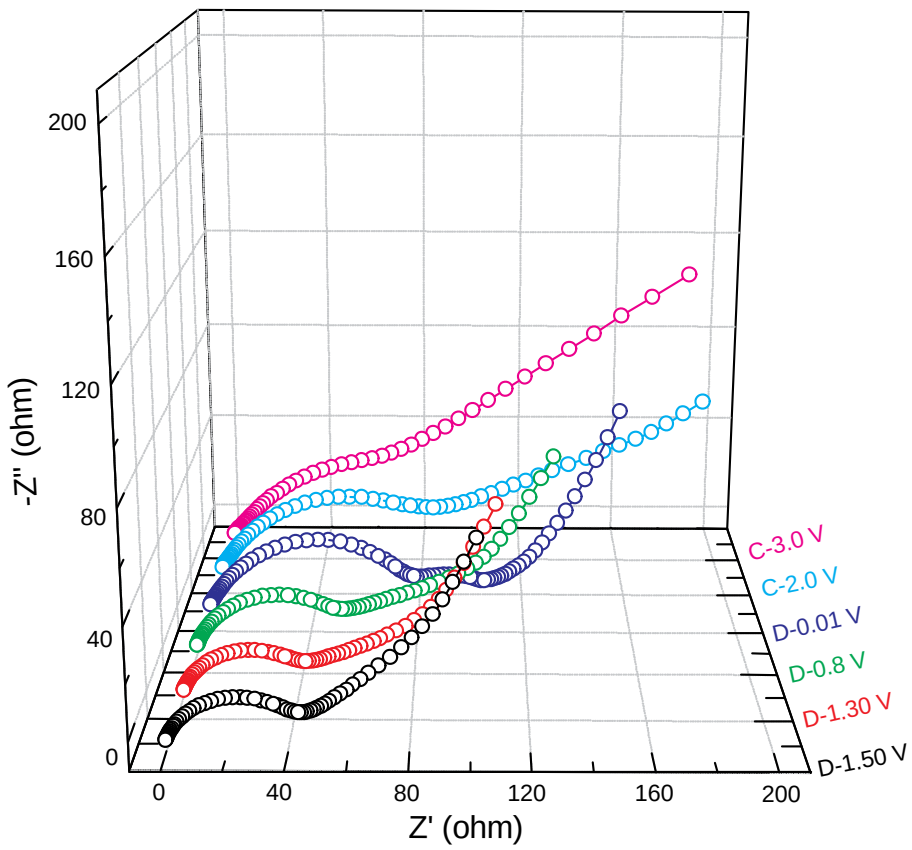

Fig. S13 Ex-situ EIS results of rGO-$FePS_3$ electrode in LIBs at selected charge-discharge states during the first cycle.

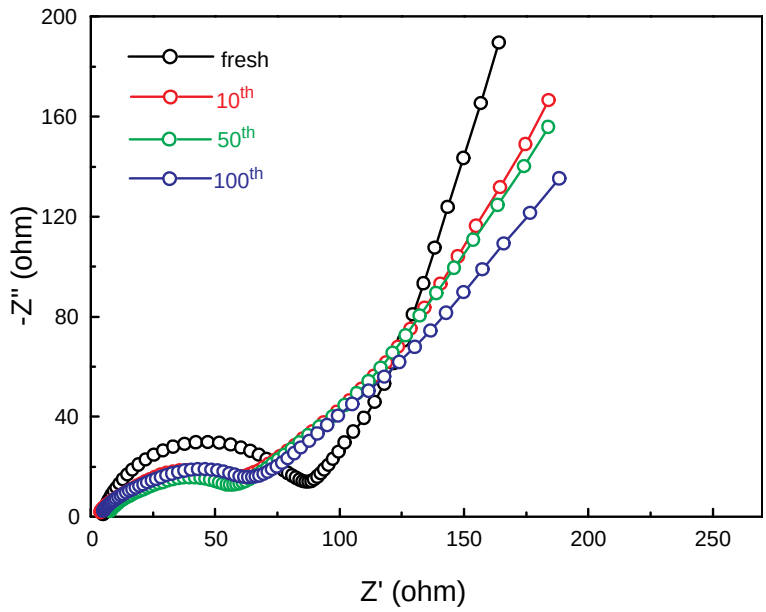

Fig. S14 EIS results of the rGO-$FePS_3$ electrode in LIBs at different cycles.

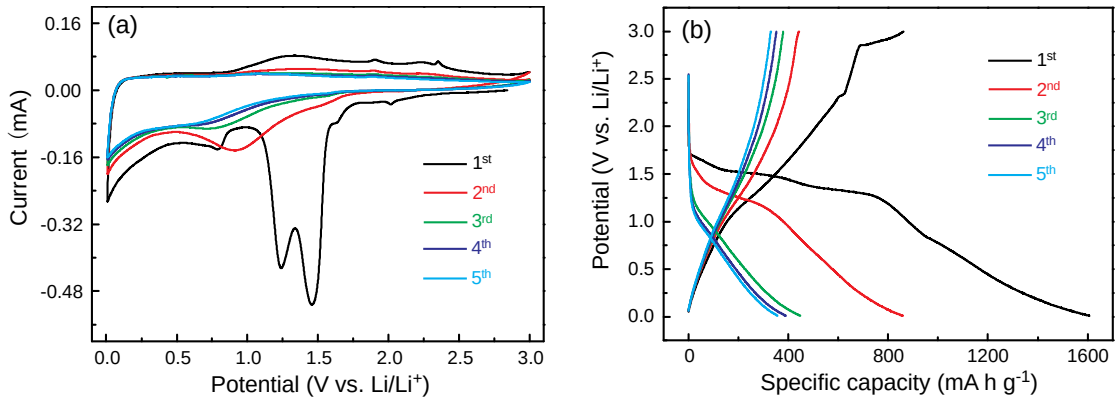

Fig. S15 (a) CV curves at the scan rate of 0.1 mV s^{-1} and (b) charge-discharge profiles at 0.1 A g^{-1} of b-$FePS_3$ electrode for LIBs at different cycles.

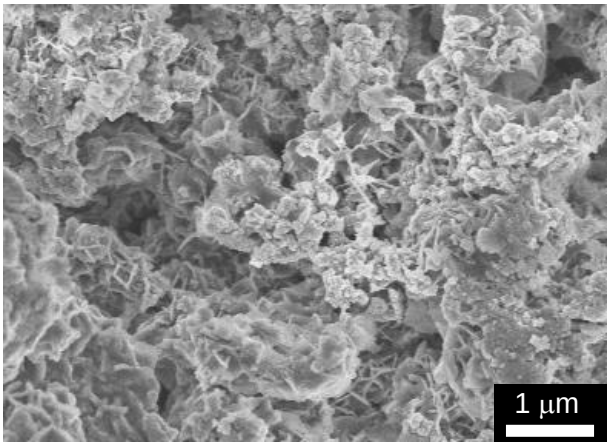

Fig. S16 SEM image of rGO-$FePS_3$ electrode after 200 cycles for LIBs.

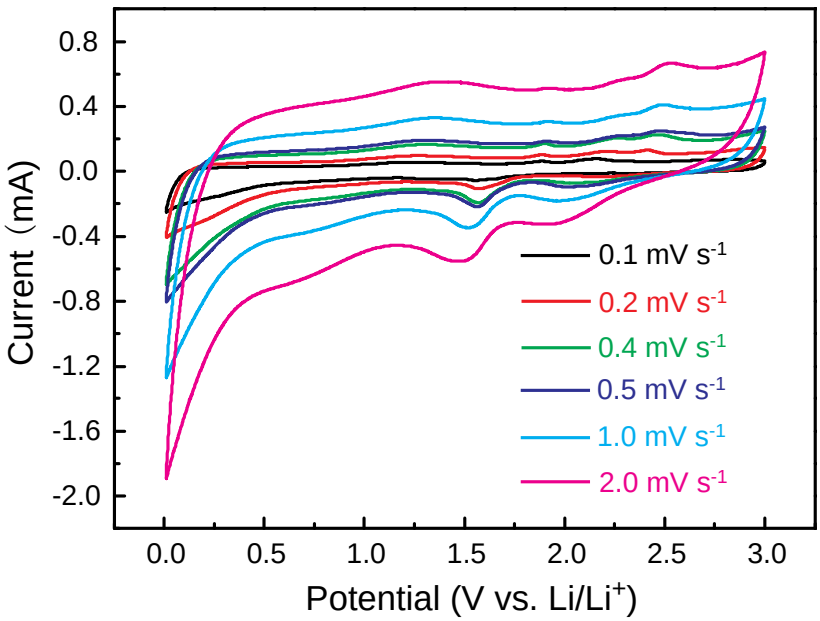

Fig. S17 The CV curves of rGO-$FePS_3$ electrode at different scan rates for LIBs.

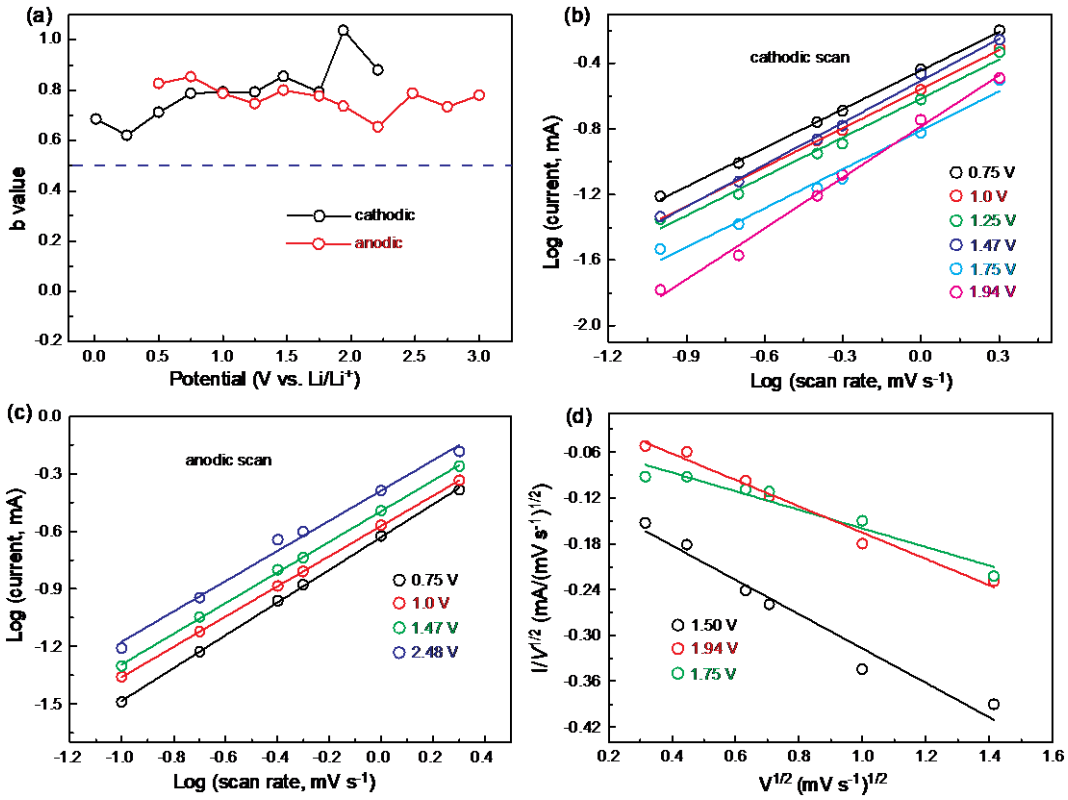

Fig. S18 (a) b value vs. battery voltage of the rGO-$FePS_3$ electrode at cathodic and anodic scans for LIBs. The representative current response plotted against scan rates at different voltages in the (b) cathodic scan and (c) anodic scan. (d) The calculated k_1 and k_2 values at different voltages in the cathodic scan. The k_1 and k_2 is acquired via plotting the $v^{1/2}$ vs. $i/v^{1/2}$ at different voltages according to the Equation:

$$i = k_1 v + k_2 v^{1/2}$$

Where k_1 and k_2 are appropriate values, $k_1 v$ is the capacitive contribution while $k_2 v^{1/2}$ corresponds to the diffusion-controlled contribution.

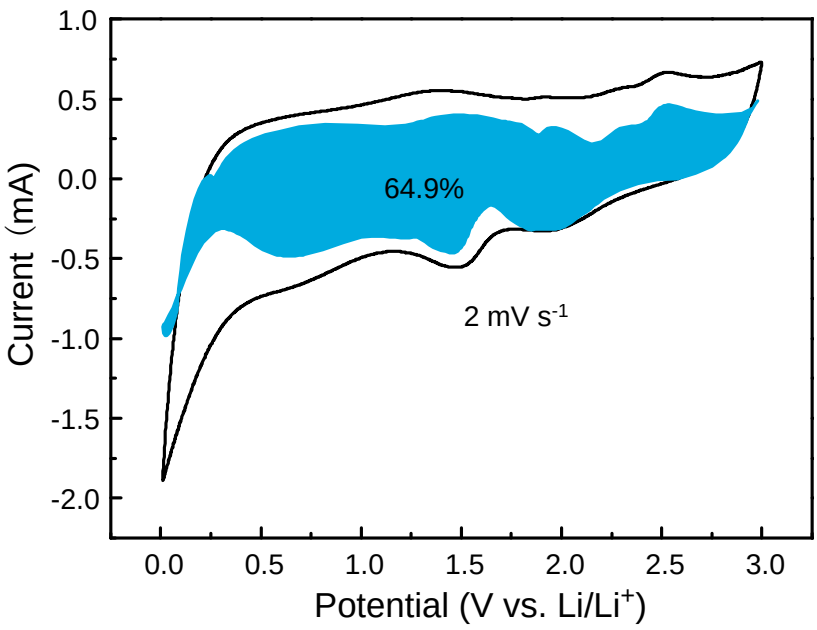

Fig. S19 The separation of capacitive contribution (blue region) from the charge storage at scan rate of 2 mV s^{-1}.

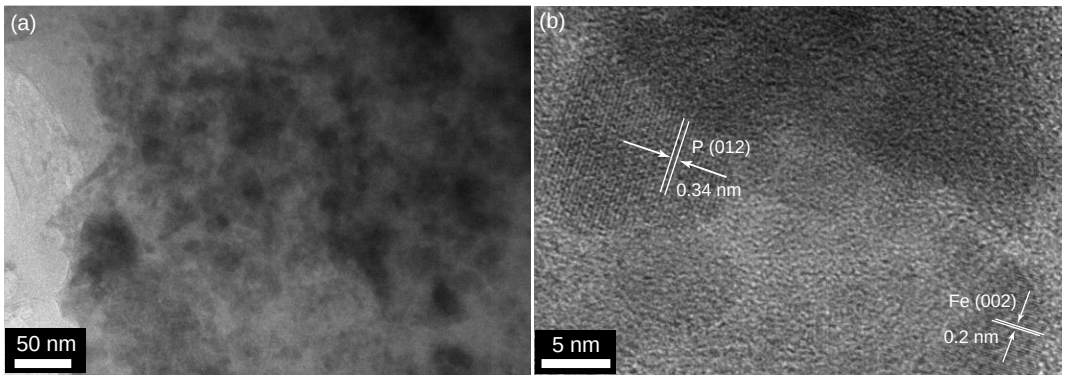

Fig. S20 (a) TEM and (b) HRTEM images of the rGO-$FePS_3$ electrode after discharging to 0.01 V for sodium storage.

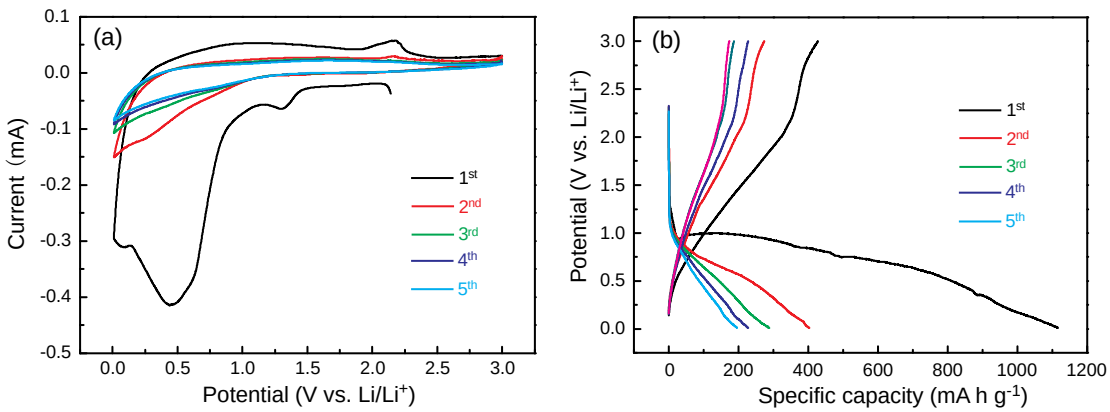

Fig. S21 (a) CV curves at the scan rate of 0.1 mV s^{-1} and (b) charge-discharge profiles at 0.05 A g^{-1} of b-$FePS_3$ electrode for SIBs at different cycles.

References

1 D. C. Marcano, D. V. Kosynkin, J. M. Berlin, A. Sinitskii, Z. Sun, A. Slesarev, L. B. Alemany, W. Lu and J. M. Tour, *ACS Nano*, 2010, **4**, 4806.

2 Y. Lu and E. Fong, *J. Mater. Chem. A*, 2016, **4**, 2738.

3 Z. Zhang, Z. Li and L. Yin, *New J. Chem.*, 2018, **42**, 1467.

4 J. Li, D. Yan, X. Zhang, S. Hou, T. Lu, Y. Yao and L. Pan, *J. Mater. Chem. A*, 2017, **5**, 20428.

5 H. Li, Y. Su, W. Sun and Y. Wang, *Adv. Funct. Mater.*, 2016, **26**, 8345.

6 Y. Jiang, Y. Guo, W. Lu, Z. Feng, B. Xi, S. Kai, J. Zhang, J. Feng and S. Xiong, *ACS Appl. Mater. Interfaces*, 2017, **9**, 27697.

7 B. Li, P. Gu, G. Zhang, Y. Lu, K. Huang, H. Xue and H. Pang, *Small*, 2018, **14**, 1702184.

8 C. Zhu, P. Kopold, W. Li, P. A. van Aken, J. Maier and Y. Yu, *Adv. Sci.*, 2015, **2**, 1500200.

9 A. A. AbdelHamid, X. Yang, J. Yang, X. Chen and J. Y. Ying, *Nano Energy*, 2016, **26**, 425.

10 Q. Tang, Y. Cui, J. Wu, D. Qu, A. P. Baker, Y. Ma, X. Song and Y. Liu, *Nano Energy*, 2017, **41**, 377.

11 X. Gao, J. Wang, D. Zhang, K. Adair, K. Feng, N. Sun, H. Zheng, H. Shao, J. Zhong, Y. Ma, X. Sun and X. Sun, *J. Mater. Chem. A*, 2017, **5**, 25625.

12 X. Wang, Z. Na, D. Yin, C. Wang, G. Huang and L. Wang, *Energy Storage Mater.*, 2018, **12**, 103.

13 M. Zhang, R. Hu, J. Liu, L. Ouyang, J. Liu, L. Yang and M. Zhu, *Electrochem. Commun.*, 2017, **77**, 85.

14 D. Yang, J. Zhu, X. Rui, H. Tan, R. Cai, H. E. Hoster, D. Y. Yu, H. H. Hng and Q. Yan, *ACS Appl. Mater. Interfaces*, 2013, **5**, 1093.

15 X. Wang, K. Chen, G. Wang, X. Liu and H. Wang, *ACS Nano*, 2017, **11**, 11602.

16 H. Guo, C. Chen, K. Chen, H. Cai, X. Chang, S. Liu, W. Li, Y. Wang and C. Wang, *J. Mater. Chem. A*, 2017, **5**, 22316.

17 C. Wu, P. Kopold, P. A. van Aken, J. Maier and Y. Yu, *Adv. Mater.*, 2017, **29**, 1604015.

18 Y. Feng, H. Zhang, Y. Mu, W. Li, J. Sun, K. Wu and Y. Wang, *Chem. Eur. J.*, 2015, **21**, 9229.

19 T. Wu, S. Zhang, Q. He, X. Hong, F. Wang, X. Wu, J. Yang and Z. Wen, *ACS Appl. Mater. Interfaces*, 2017, **9**, 28549.
20 Z. Cao, H. Song, B. Cao, J. Ma, X. Chen, J. Zhou and Z. Ma, *J. Power Sources*, 2017, **364**, 208.
21 S. Dong, C. Li, X. Ge, Z. Li, X. Miao and L. Yin, *ACS Nano*, 2017, **11**, 6474.
22 X. Song, X. Li, Z. Bai, B. Yan, D. Li and X. Sun, *Nano Energy*, 2016, **26**, 533.
23 R. Sun, Q. Wei, J. Sheng, C. Shi, Q. An, S. Liu and L. Mai, *Nano Energy*, 2017, **35**, 396.
24 H. Li, Y. Su, W. Sun and Y. Wang, *Adv. Funct. Mater.*, 2016, **26**, 8345.
25 D. Lan, W. Wang and Q. Li, *Nano Energy*, 2017, **39**, 506.
26 D. Zhou and L.-Z. Fan, *J. Mater. Chem. A*, 2018, **6**, 2139.
27 Z. Li, L. Zhang, X. Ge, C. Li, S. Dong, C. Wang and L. Yin, *Nano Energy*, 2017, **32**, 494.
28 S. Huang, C. Meng, M. Xiao, S. Ren, S. Wang, D. Han, Y. Li and Y. Meng, *Sustainable Energy Fuels*, 2017, **1**, 1944.
29 X. Ge, Z. Li and L. Yin, *Nano Energy*, 2017, **32**, 117.
30 Z. Huang, H. Hou, C. Wang, S. Li, Y. Zhang and X. Ji, *Chem. Mater.*, 2017, **29**, 7313.